Journal of Drug Delivery Science and Technology 81 (2023) 104304

Contents lists available at ScienceDirect

Journal of Drug Delivery Science and Technology

journal homepage: www.elsevier.com/locate/jddst

Research paper

Improving quercetin anticancer activity through a novel polyvinylpyrrolidone/polyvinyl alcohol/TiO_2 nanocomposite

Mohammad Mahdi Eshaghi [a], Mehrab Pourmadadi [a], Abbas Rahdar [b,**], Ana M. Díez-Pascual [c,*]

[a] Department of Biotechnology, School of Chemical Engineering, College of Engineering, University of Tehran, Tehran, Iran
[b] Department of Physics, Faculty of Sciences, University of Zabol, Zabol, 538-98615, Iran
[c] Universidad de Alcalá, Facultad de Ciencias, Departamento de Química Analítica, Química Física e Ingeniería Química, Ctra. Madrid-Barcelona, Km. 33.6, 28805, Alcalá de Henares, Madrid, Spain

ARTICLE INFO

Keywords:
TiO_2
Nanocarrier
Drug delivery
Cancer therapy
Quercetin

ABSTRACT

A hydrogel nanocomposite comprising polyvinylpyrrolidone (PVP), polyvinyl alcohol (PVA), and titanium oxide (TiO_2) was prepared and encapsulated in a double emulsion as a pH-triggered delivery vehicle for quercetin (QC), an antitumor drug. Dynamic light scattering (DLS) was used to estimate the size and confirm the stability of QC-loaded nanoparticles. The interactions between the nanocomposite components, its crystalline structure and the morphology of the nanoparticles were characterized through Fourier transform infrared (FTIR) spectroscopy, X-ray diffraction (XRD) and field emission scanning electron microscopy (FESEM), respectively. Drug loading and encapsulation efficiency significantly improved after incorporation of TiO_2, which corroborates the beneficial effect of this component. *In vitro* release experiments indicated the pH-responsivity of the nanocarrier, with higher amount of QC released in an acidic medium than at neutral pH. Due to the presence of a double emulsion, the release pattern was sustained and gradual in both environments. Cellular experiments including MTT assay and flow cytometry were conducted using U87 cell line to compare the anticancer activity of free QC and QC-loaded nanoparticles. MTT assay was also performed on a noncancerous cell line (L929) to assess potential side effects of the drug release system. The results obtained herein confirm the suitability of the developed nanocarrier as an efficient drug delivery vehicle for tumor therapy.

1. Introduction

According to statistics, cancer is the second most fatal disease in the USA. A total of 1.9 million new cancer cases and 609,360 deaths occurred in 2022, which is about 1670 deaths a day [1]. Traditional approaches towards cancer therapy such as chemotherapy suffer drawbacks like drug resistance, low bioavailability, non-specific targeting, uncontrolled release, and insufficient solubility. One solution that has been widely explored to tackle these problems is the use of smart nanoplatforms for drug delivery [2,3]. In particular, natural nanomaterials are being widely investigated as they demonstrate less side effects [4].

Flavonoids are natural polyphenolic compounds with confirmed antitumor activities. Their capability in modulating cell replication and apoptosis has been validated. Quercetin (QC) belongs to this group and is found in fruits and vegetables. Its potential to inhibit interactions between free radicals and low-density lipoproteins has been proven. This feature makes QC a potential medicine for cancer treatment. Other beneficial properties of QC include antiviral, antidiabetic, and anti-inflammatory activity [5–9]. Despite the advantages of natural products like QC for cancer therapy, drawbacks such as low aqueous solubility and bioavailability hinder their efficient antineoplastic activity [4]. Tackling these issues through encapsulation of the drug in polymeric nanocarriers have been extensively investigated in the last two decades [10].

Hydrogels are networks made of crosslinked polymers with hydrophilic functional groups that enable to absorb large amounts of water. Polymeric hydrogels as drug carriers offer several benefits including low cytotoxicity and favorable biocompatibility. High swelling capacity, softness, and flexible structure allows hydrogels to mimic structural

* Corresponding author.
** Corresponding author.
E-mail addresses: mohammadeshagi3782@gmail.com (M.M. Eshaghi), mehrabpourmadadi@gmail.com (M. Pourmadadi), a.rahdar@uoz.ac.ir (A. Rahdar), am.diez@uah.es (A.M. Díez-Pascual).

https://doi.org/10.1016/j.jddst.2023.104304
Received 8 November 2022; Received in revised form 9 February 2023; Accepted 22 February 2023
Available online 28 February 2023

properties of body components [11–14]. Regarding the choice of building blocks for the polymeric hydrogel, natural polymers like chitosan show advantages like biocompatibility and biodegradability. However, low mechanical properties can compromise their role as drug carriers *in vivo*. Synthetic polymers such as polyvinyl alcohol (PVA) and polyvinylpyrrolidone (PVP) are a suitable alternative to natural macromolecules owed to their good chemical and physical properties [15], including biocompatibility, water-solubility, thermal and chemical stability, making them ideal candidates for developing hydrogel nanocarriers [16]. The combination of PVA and PVP leads to a new hydrogel structure with improved features compared to the pure components due to synergistic effects. The interconnected network comprising both polymers is the result of hydrogen bonds formed between hydroxyl groups of PVA and carbonyl groups of PVP, which increase polymer stability and prevents PVA degradation [17]. Further, an interlocked network of PVP and PVA contributes to decrease burst release.

Stimuli can significantly enhance the therapeutic efficiency of drug carriers as they aid to release their payload at the site of interest and not toward healthy tissues. Among factors that can trigger drug release are light, pH, temperature, sound waves, magnetic field, etc. To be considered stimuli-responsive, the nanocarrier structure needs to change upon modification of one of the mentioned factors. These structural changes can facilitate the release of the cargo at the required site and prevent its accidental release in other parts of the body [18–20]. One of the most suitable stimuli for cancer therapy is pH, since the pH of tumor microenvironment is noticeably lower than that of healthy tissues; therefore, using pH-triggered nanocarriers is a smart approach for enhancing therapeutic effects of antitumor drugs [21,22]. Several works have been reported regarding the successful development of pH-responsive drug carriers for improving drug delivery efficacy. Madhusudana and coworkers [23] developed a pH-sensitive polymeric nanogel loaded with curcumin, which released higher amount of the drug in a neutral environment than in an acidic one. However, stimuli-responsive hydrogels have the limitation of lengthy response time which compromises delivery efficacy [24]. Also, they suffer from low mechanical strength which causes structural collapse [25], large pore size [26], and high swelling degree [27], leading to burst release of the payload. Moreover, hydrophobic drugs cannot be loaded in hydrogels in large quantities due to the aqueous nature of the hydrogels [27]. Incorporating inorganic nanoparticles such as metal oxides within the hydrogel network can improve its mechanical strength, biocompatibility, biodegradability, swelling rate and provide it with more functions [28]. Literature reports have revealed the potential of titanium oxide (TiO_2) nanoparticles as a pH-responsive carrier for drugs. Zhang and coworkers [29] reported the fabrication of a pH-sensitive nanocomposite composed of TiO_2 nanoparticles and daunorubicin drug. Their release studies indicated that protonation of daunorubicin molecules at acid pH along with shifting of TiO_2 surface charge to positive values led to dissociation of the drug from the inorganic nanocarrier. Features such as pH-sensitivity and high surface area of TiO_2 nanoparticles can lead to higher drug uptake, increased loading capacity for hydrogels, and improved performance of the therapeutic cargo [30–32].

In this study, a hydrogel nanocomposite comprising PVP, PVA, and TiO_2 nanoparticles for QC delivery has been synthesized. Successful incorporation of QC within the PVP/PVA polymeric network can be associated with the hydrogen bonds formed between phenolic groups of the drug with C═O groups of PVP and O–H groups of PVA, as reported in the literature [33,34]. Moreover, interactions between PVA and TiO_2 nanoparticles have been reported by Ahmad et al. [35] which proves feasibility of incorporating TiO_2 nanoparticles within PVA network. These interactions along with the large surface area of TiO_2 nanoparticles improve the encapsulation efficiency of QC. At lower pH values, the protonation of C═O groups of PVP, O–H groups of PVA, and O–H groups of QC disrupts the abovementioned interactions and creates a repulsive electrostatic force between the molecules. Hence the structure of the nanocomposite is compromised and higher amounts of QC are released compared to neutral conditions [36].

Following the synthesis of the hydrogel nanocomposite, a water-in-oil-in-water double emulsion was prepared according to the method reported by Chouaibi and colleagues [37]. Multiple layers of the double emulsion system can increase the release time and develop a sustained release profile for QC. Slow and sustained release profile is of paramount importance for drugs such as QC that have low bioavailability. The oil layer that separates the two water layers controls the release rate of the drug [38,39]. A hydrophobic and hydrophilic surfactant are used in the two respective steps of preparing the emulsion to facilitate interactions between the initial aqueous interface and the oil interface, and the interactions between the dispersed oil phase and the outer aqueous phase [36].

To sum up, the purpose of this study was to prepare a hydrogel nanocomposite of PVP/PVA/TiO_2 loaded with QC and entrapped in the inner aqueous layer of a double emulsion system. To the best of our knowledge, no previous study has used such formulation for drug delivery purposes. The nanocarrier displayed high loading efficiency and pH-sensitivity feature, which would facilitate controlled release of the therapeutic payload. The cytotoxicity of the developed system on U-87 cell line was investigated to evaluate its therapeutic efficiency for cancer. The same study was conducted on L929 cell line to assess potential side effects induced by the nanocarrier.

2. Materials and methods

2.1. Materials

Phosphate-buffered saline (PBS), PVA $(C_4H_6O_2)_n$, 87–90% hydrolyzed, $d_{25°C}$ = 1.19–1.31 g/cm^3, average Mw = 30000–70000), PVP ($(C_6H_9NO)_n$, $d_{25°C}$ = 1.20 g/cm^3, average Mw = 40000), TiO_2 nanoparticles (10% wt. in ethanol, <150 nm particle size), QC drug ($C_{15}H_{10}O_7$, Mw = 302.24 g/mol, >95% (HPLC), solid) and ethyl acetate (anhydrous, 99.8%) were purchased from Sigma Aldrich Co. SPAN 80 ($C_{24}H_{44}O_6$, Mw = 428.60 g/mol) was obtained from Merck Co.

2.2. Preparation of PVP/PVA/TiO_2/QC nanocomposite

Firstly, 0.4 g of PVP was added to 20 mL of 2% (v/v) acetic acid solution and the resulting mixture was placed on heater stirrer at room temperature until a homogenous PVP solution of 2% (w/v) was achieved. This was followed by addition of 0.2 g PVA powder to the obtained mixture. After mechanical stirring and complete homogenization, the resulting solution of PVP and PVA was placed in an ultrasonic bath for 10 min. In the next step, 20 mg of TiO_2 nanoparticles were added to the magnetically stirred solution until the nanoparticles were completely dispersed in the polymeric network [37]. The amount of QC loaded on the hydrogel was chosen in order to attain a final concentration of the drug in the hydrogel of 5 μg/mL. After 30 min on the heater stirrer, a uniform PVP/PVA/TiO_2/QC hydrogel was obtained.

2.3. Preparation of PVP/PVA/TiO_2/QC double emulsion

The double emulsion system was prepared following a procedure similar to that reported earlier [22]. Firstly, 20 mL of the QC-loaded hydrogel was extracted using a syringe. The extract was added dropwise to 60 mL of nigella sativa oil containing 2% (v/v) SPAN 80 under continuous stirring. Thus, spherical QC-loaded nanocarriers were formed within the lipophilic phase. After 10 min of stirring, 20 mL of distilled water was added to the nigella sativa oil which acted as the outer hydrophilic layer. The resulting emulsion system was stirred for another 10 min and then the solution was kept undisturbed for 10 min so that the layers separated from each other. Finally, a sampler and a centrifugation (4500 rpm, 10 min) were used to remove the lipophilic and aqueous phase, respectively. Drying of the samples was performed using a freeze dryer. The samples were first frozen at −20 °C and then

dried by means of a freeze dryer.

2.4. Characterization of the nanocomposite

The surface morphology of the developed nanocarrier was examined using a field emission scanning electron microscopy (FESEM: Quanta, FEG 250, Japan), operating at a voltage of 20 kV. The size and stability of the nanoparticles was measured by means of dynamic light scattering (DLS) technique and zeta potential measurements using a Zetasizer Nano (Malvern, UK). Fourier transform infrared (FTIR) spectroscopy was used to get insight about the interactions between the nanocomposite components. Spectra were recorded using an Alpha Platinum FTIR spectrophotometer (Bruker, MA, USA) equipped with an attenuated total reflection (ATR) accessory, in the wavenumber range of 4000-500 cm^{-1}. The crystalline nature of the nanocomposite and the modifications of its structure after addition of each component were studied using X-ray diffraction (XRD) analysis with a D2 Phaser diffractometer (Bruker, MA, USA) in the 2θ range from 5 to 80°.

2.5. Drug loading and encapsulation efficiency

The loading and encapsulation efficiency of both PVP/PVA/QC and PVP/PVA/TiO_2/QC nanoparticles were determined to assess the impact of incorporating the inorganic nanoparticles in the polymeric structure. For such purpose, the samples were added to PBS. Next, ethyl acetate was added to the mechanically agitated solution until a homogenous mixture was obtained. The organic phase was then removed and its quercetin content was measured using a UV–Vis spectrophotometer. A linear correlation between optical density and amount of free drug was obtained. Equation (1) and were used to calculate loading efficiency and encapsulation efficiency, respectively.

$$Loading\ efficiency\ (\%) = \frac{Total\ QC\ quantitiy - Free\ QC\ quantitiy}{Total\ nanocarrier\ quantity} \quad (1)$$

$$Encapsulation\ efficiency\ (\%) = \frac{Total\ QC\ quantitiy - Free\ QC\ quantitiy}{Total\ QC\ quantity} \quad (2)$$

2.6. In vitro drug release

The release profile of the payload was simulated in vitro through dialysis bag method [36]. In this regard, a beaker was filled with water (37 °C) to mimic the thermal conditions of the body. The beaker was placed on a stirrer to ensure uniform temperature throughout the beaker. Two Falcon test tubes were filled with PBS containing 20% (v/v) ethanol at pH values of 7.4 and 5.4 which correspond to the microenvironment of healthy and tumor-containing tissues, respectively. Afterwards, the tubes were immersed within the water-containing beaker. Next, two dialysis bags containing QC-loaded nanoparticles were placed within the Falcon test tubes. While the PBS containing tubes are meant to represent tissue environment, the porous dialysis bags represent veins in which nanoparticles flow. Samples were taken from the test tubes 0, 0.5, 1, 2, 3, 6, 12, 24, 48, 72, and 96 h after the beginning of the experiment. In each turn of sample extraction, proportional quantity of fresh PBS was added to the tubes. The portion of released QC was then measured by means of UV–Vis light and the release percentage was calculated using equation (3).

$$Released\ QC\ percentage = \frac{Released\ QC}{Loaded\ QC} \times 100 \quad (3)$$

In equation (3), "Loaded QC" is the initial amount of drug loaded on the nanoparticles and "ReleasedQC" is the amount of drug within the extracted samples, which was measured using a UV–Vis spectrophotometer.

2.7. Cell culture

U87 cell line (cancerous cell line, human glioblastoma) was cultured in RPMI-1640 medium (deprived of folate) at 37 °C, containing 0.5% CO_2. This cell line was used in MTT assay and flow cytometry test to assess the antitumor activity of the nanoparticles. L929 fibroblast cell line was cultured in RPMI-1640 medium under the same conditions as U87 cells. Cellular tests were performed using L929 cells estimate the potential cytotoxic effect of nanoparticles on healthy cells. Both cell lines were provided by Pasteur Institute (Tehran, Iran).

2.8. MTT assay

An MTT assay was applied to evaluate cytotoxic behavior of free QC, PVP, PVP/PVA, PVP/PVA/TiO_2, and PVP/PVA/TiO_2/QC against both U87 and L929 cell lines. Culture mediums containing 10^4 cells were used to fill wells of a 96-well plate. Following one day of incubation to achieve desirable cell adhesion, both cell lines were treated with each of the mentioned samples for 24 h. The reason for testing the mentioned samples was to inspect the cytotoxic effects of each component on the cells. Also, a control group of cells were prepared using the same medium (RPMI-1640). Optical density values were measured through an ELISA reader and the cell viability percentage was calculated with respect to the control group. All the experiments were repeated three times and the results are presented as mean ± standard error of the mean (SEM).

2.9. Flow cytometry test

To further verify the results of MTT assay, flow cytometry test was performed using U87 cell line to determine the share of apoptotic and necrotic death induced by free QC, PVP, PVP/PVA, PVP/PVA/TiO_2, and PVP/PVA/TiO_2/QC. The cells were treated with each sample for 24 h, and then washed with PBS. A suspension of cells was then formed in a binding buffer and the cells were stained using Annexin V-FITC. By analyzing the fluorescence intensity using a flow cytometer, the share of cells with necrotic death (Q1), late apoptotic death (Q2), early apoptotic death (Q3), and viability (Q4) were determined. Each test was repeated three times.

3. Results and discussions

3.1. DLS

The size and zeta potential of PVP/PVA, PVP/PVA/TiO_2 and PVP/PVA/TiO_2/QC nanoparticles was assessed by means of DLS technique, and the results for each of the abovementioned formulations are shown in Figs. 1–3. PVP/PVA nanoparticles have and average size of 119 nm and average zeta potential of 31 mV (Fig. 1). The addition of TiO_2 nanoparticles increases the average size to 300 nm and the zeta potential by 7 mV (Fig. 2). Once QC is entrapped in the nanocarrier, the average size rises to 330 nm and mean zeta potential reaches 51 mV (Fig. 3). The size of the nanoparticles increases with the addition of each component within the polymeric network, which is reasonable and validates the effectiveness of the synthesis protocol. According to literature, zeta potential values above 30 mV are indicative of good particle stability [40]. A high value of zeta potential indicates large surface charge of the particles that hinders their aggregation through repulsive electrostatic forces.

Regarding DLS tests over time at different pH (7.4 and 5.4), a previous work by El-Rehim et al. [42] has proven the pH-sensitivity of PVP involved in a copolymer network. Also, the studies of Liu and coworkers [43] using DLS verified the pH-sensitivity of PVA in copolymeric nanoparticles. In both studies, the copolymer comprised either PVP or PVA and poly acrylic acid. To verify the pH-sensitivity of PVP/PVA/TiO_2 nanoparticles, DLS test was replaced herein by a dialysis bag experiment

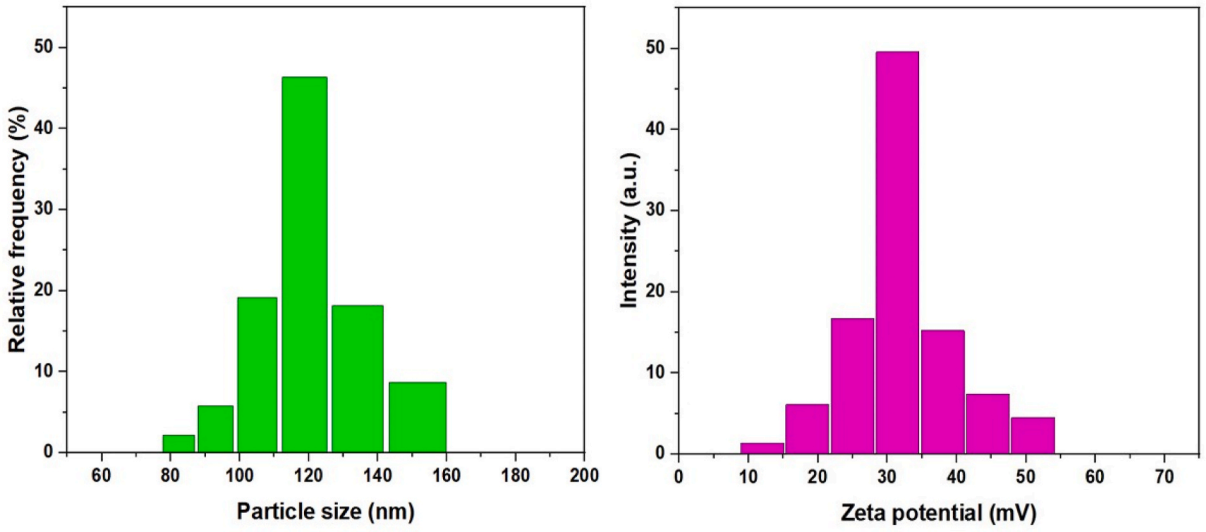

Fig. 1. Size and zeta potential distribution of PVP/PVA nanoparticles determined by DLS. Average size: 119 nm, Average zeta potential: 31 mV.

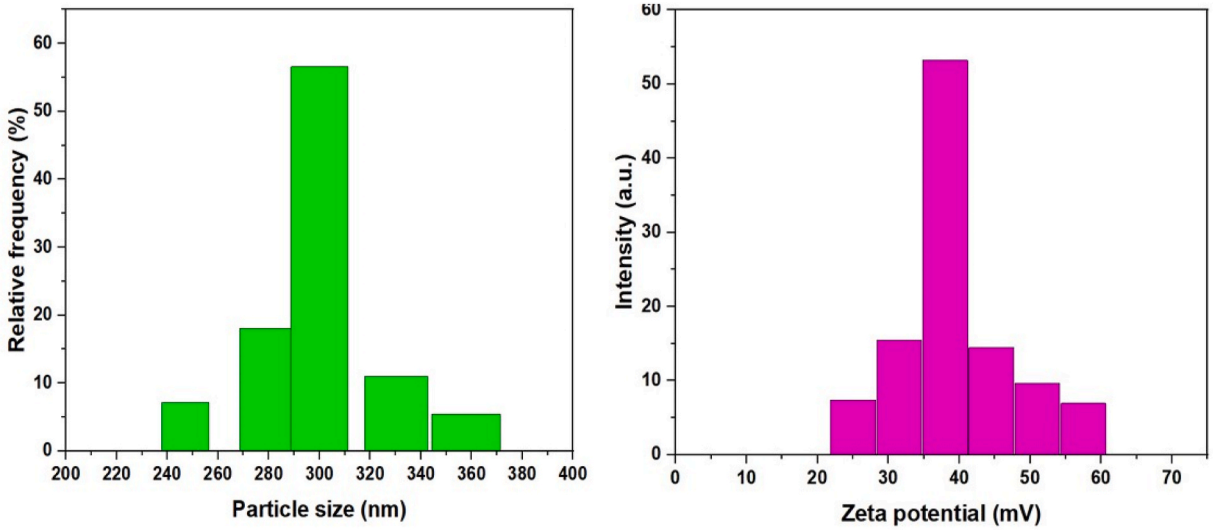

Fig. 2. Size and zeta potential distribution of PVP/PVA/TiO_2 nanoparticles. Average size: 300 nm, Average zeta potential: 38 mV.

to mimic the thermal conditions of the body (37 °C), and the nanoparticles were separated from the simulated tissue microenvironment (PBS solution) using a porous dialysis bag (as blood vessels). Our experiment confirmed the pH-sensitivity of the nanoparticles.

3.2. FE-SEM

FESEM was used to get insight about the surface morphology and state of dispersion of the nanoparticles in the nanocomposite, and representative micrographs at two different scales (20 μm and 500 nm) are shown in Fig. 4. These images illustrate an interconnected structure comprising the polymeric fibers of the synthesized nanocomposite loaded with QC. As can be visualized in the micrographs, the polymeric fibers have a uniform size distribution and a smooth surface, indicating good compatibility between the building units of the nanocomposite (PVP, PVA, and TiO_2), which can be attributed to strong chemical interactions between these components that lead to the formation of an integrated network. These interactions are discussed in more detail in section 3.3.

Measurements in different sections of the image revealed sizes in the range of 110-75 nm. There are significant differences between the sizes obtained by FESEM and DLS. The lower particle size obtained by SEM imaging can be attributed to the fact that DLS relies on Rayleigh scattering from nanoparticles dispersed in a liquid that undergo Brownian motion. By illuminating the sample with a laser source to estimate the diffusion speed of the particles, the hydrodynamic diameter of the nanoparticles can be calculated. However, it includes hydration layer, polymer shells or other possible stabilizers, leading to a larger particle size. It also assumes that there is no interaction between particles that are treated as uniform isotropic non-interacting single scattering spheres. On the other hand, SEM is a powerful technique to resolve different particle sizes in the solid state. When comparing the results from the SEM images, it has to be taken into account that the hydrated polymeric shell collapses during drying and in the high vacuum chamber of the SEM.

Similar differences in size using SEM and DLS techniques have been previously reported for other nanocomposites such as carboxymethyl cellulose (CMC)-based hydrogels designed for QC delivery [44]. Overall, SEM seems a more reliable technique to assess the state of dispersion of the nanoparticles in the nanocomposite, and according to the observed images, there is a uniform distribution of the synthesized fibers loaded with QC.

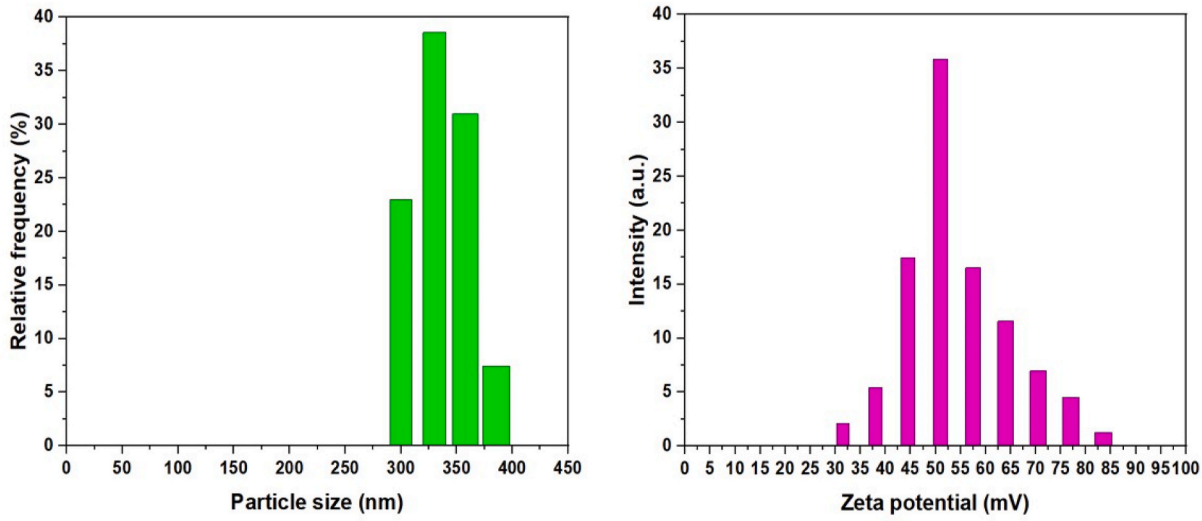

Fig. 3. Size and zeta potential distribution of PVP/PVA/TiO_2/QC nanoparticles. Average size: 330 nm, Average zeta potential: 51 mV.

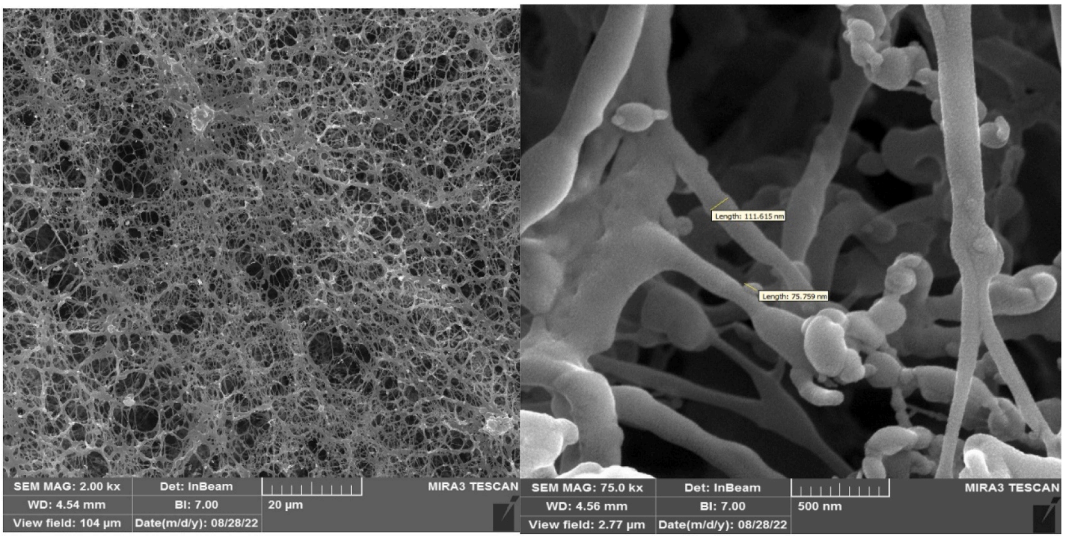

Fig. 4. FESEM images of PVP/PVA/TiO_2/QC nanomulsions with two scales: 20 µm, 500 nm (from left to right).

3.3. FTIR

FTIR analysis was performed for get information about the functional groups of the different samples and the interactions between these functional groups upon mixing the components, and the results are shown in Fig. 5. Regarding the spectrum of neat PVA, the peak at 3379 cm^{-1} is related to the O–H stretching and those at 2940 cm^{-1} and 956 cm^{-1} correspond to C–H asymmetric and CO symmetric stretching, respectively. The characteristic C═O stretching appears at 1715 cm^{-1}. The peak located at around 1570 cm^{-1} corresponds to C–H and O–H bending vibrations, and the C–H bending of the CH_2 groups appear at 1242 cm^{-1} (wagging) and 848 cm^{-1} (rocking). In the FTIR spectra of PVP, the O–H stretching is observed at 3461 cm^{-1}. Moreover, C–N and C═O stretching appear at 2127 cm^{-1} and 1666 cm^{-1}, and the CH_2 rocking at 875 cm^{-1}. In the crosslinked network composed of PVP and PVA (PVP/PVA), hydrogen bonds are formed between C═O groups of PVP and O–H groups of PVA. The O–H stretching appears at 3496 cm^{-1}, the asymmetric C–H stretching of CH2 at 2924 cm^{-1} and the symmetric stretching of C═O at around 948 cm^{-1}. Further, peaks located between 1600 and 1700 cm^{-1} can be assigned to C═C stretching vibrations of polaronic states, in agreement with previous literature reports [41].

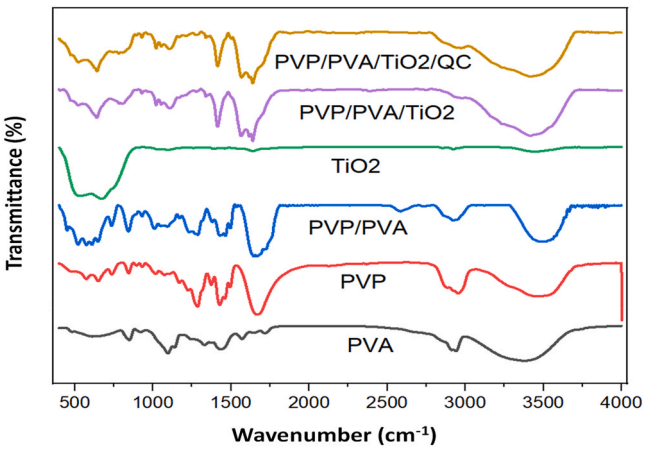

Fig. 5. FTIR spectra of PVA, PVP, PVP/PVA, TiO_2, PVP/PVA/TiO_2, and PVP/PVA/TiO_2/QC.

Regarding TiO_2 spectra, the peak observed at 605 cm^{-1} corresponds to the vibration of Ti–O bond, in agreement with results reported earlier [42]. Upon incorporation of TiO_2 within the polymeric network of PVP/PVA, all the characteristic peaks of the components can be identified. Moreover, the intensification of the peak located at around 3500 cm^{-1} can be associated with the interaction between O–H groups of PVA, C═O groups of PVP, and TiO_2 nanoparticles. Similar interactions related with the corresponding peak have been reported in the literature [43]. It is evident from Fig. 5 that loading QC within the nanocomposite network hardly modifies the position or the intensity of the peaks found in the neat nanocomposite. A slight increase in the peak located at around 1600 cm^{-1} can be associated with the overlapping of the C═O stretching for both QC and PVP which results in increased peak intensity. Also, the interactions between hydroxyl groups of QC and TiO_2 nanoparticles lead to slightly increased intensity of the peak at 3500 cm^{-1}.

3.4. XRD

XRD analysis was employed to determine the crystalline structure of each component of the nanocarrier. The diffractograms for PVA, PVP, PVP/PVA, TiO_2, PVP/PVA/TiO_2 and PVP/PVA/TiO_2/QC are shown in Fig. 6. In the pattern of PVA, an intense peak is observed at 19.75°, corresponding to (110) plane [47], and the semi-crystalline nature of polymer is corroborated. Regarding PVP, two weak peaks located at around 10.2 and 24.15° are indicative of the amorphous structure of the polymer [44]. The significant decrease in the intensity of PVA peak upon crosslinking of PVA and PVP and the formation of a broader peak indicates the good miscibility of the two polymers. Regarding TiO_2, several peaks are located at around 25, 36, 37, 38, 48, 53, 55, and 62°, in agreement with literature reports on XRD analysis of TiO_2 nanoparticles, and confirm its anatase crystalline structure [45]. It is evident from Fig. 6 that all the peaks of TiO_2 either vanish or lose intensity upon incorporation of TiO_2 nanoparticles within the polymeric network. This result confirms the successful incorporation of the inorganic nanoparticles within the polymeric hydrogel and the reduced or vanished intensities represent the formation of a complex between TiO_2 and the amorphous network of PVP/PVA. QC has a crystalline structure [46]. However, the diffractogram for the QC loaded-nanocomposite does not show any additional peak related to QC, which is an indication of the effective loading of QC within the PVP/PVA/TiO_2 nanocomposite and the formation of a complex between QC and the nanocomposite.

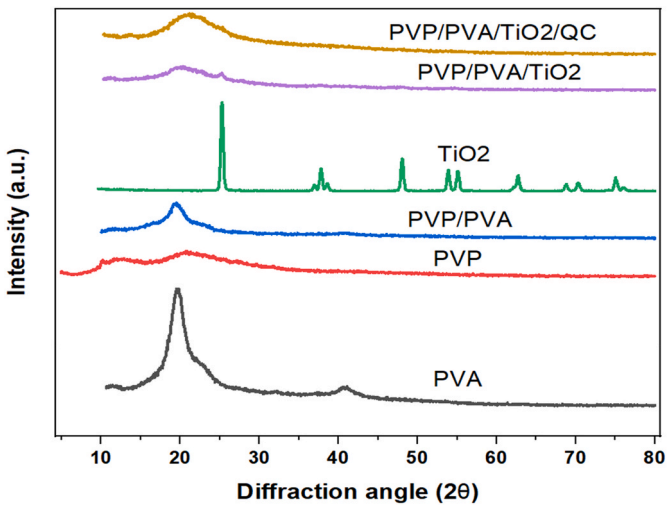

Fig. 6. Diffractograms obtained from XRD analysis for PVA, PVP, PVP/PVA, TiO_2, PVP/PVA/TiO_2 and PVP/PVA/TiO_2/QC.

3.5. Loading and encapsulation efficiency

As mentioned earlier, low solubility of QC causes its biological half-life to be very short which compromises its therapeutic efficiency. In light of this fact, improving loading and encapsulation efficiency of QC in nanocarriers is one of the major fields on which the research is focused. Herein, the loading and encapsulation efficiency for PVP/PVA hydrogel and TiO_2-containing PVP/PVA hydrogel were calculated to assess the effect of including inorganic nanoparticles within the polymeric network. For PVA/PVP, the calculated values were 44 and 85%, respectively (Table 1). Upon incorporation of TiO_2, these values increased to 48 and 89%. As explained in FTIR analysis section, the improvement in loading and encapsulation efficiency percentages after adding inorganic nanoparticles to the system can be associated with strong interactions between the O–H groups of PVA and QC, C═O groups of PVP, and TiO_2 nanoparticles. These intense interactions form an interconnected network, well suited for loading the drug. Besides the chemical interactions, the high surface area of TiO_2 is another factor contributing to an improved loading and encapsulation of QC. This high surface area provides more space for interactions between the nanocomposite components and QC.

3.6. In vitro release profile

Dialysis experiment was performed to examine the release profile of QC in both acidic and neutral environments and determine the pH-responsivity of PVP/PVA/TiO_2 nanocarriers. Fig. 7 shows the curves for cumulative released amount of QC from the synthesized nanoparticles in a 96 h-long experiment at 37 °C. PBS with acidic (pH = 5.4) and neutral (pH = 7.4) pH values were prepared to simulate the microenvironment of tumor-bearing and normal tissues, respectively. After 12 h, the cumulative release percentage of QC in acidic and neutral medium were 45 and 33%, respectively. Comparing with other literature reports on QC [47–49], this was a more sustained release pattern, which is crucial for the applicability of this nanocarrier for QC delivery. This is because the QC-loaded nanocarriers will pass through several neutral microenvironments before reaching the cancerous tissue site. Taking this into account, retaining a major amount of the therapeutic payload by the nanocarrier prior to reaching tumors is of paramount importance for guaranteeing therapeutic efficiency and reduced side effects of QC. The interconnected network (discussed in section 3.5) that the components of the designed nanocomposite create for QC are responsible for preventing undesired release of the drug in neutral environment.

Moreover, the obvious difference between the amount of QC released at different periods proves the pH-sensitivity of the drug delivery system. After 10 h, the amount of QC released in an acidic medium is higher than that released in a neutral medium at any time period until 96 h. Within the first 24 h, 43 and 57% of QC was released in neutral and acidic media, respectively. At low pH values, protonation of carbonyl and hydroxyl groups which form the hydrogen bonds between PVP, PVA, and QC leads to dissociation of these bonds and enhanced release of the drug [50]. By the end of the monitoring period (96 h), 91 and 96% of QC was released from the nanoparticles in neutral and acidic solutions, respectively.

Furthermore, entrapping the QC-loaded nanoparticles within the water-in-oil-in-water emulsion further contributes to preventing burst release and obtaining a gradual profile. The oil layer of the emulsion

Table 1
Loading and encapsulation efficiency of the nanocarriers before and after including TiO_2 nanoparticles within the polymeric network of PVP/PVA.

Hydrogel structure	Encapsulation efficiency (%)	Loading efficiency (%)
PVP/PVA	85	44
PVP/PVA/TiO_2	89	48

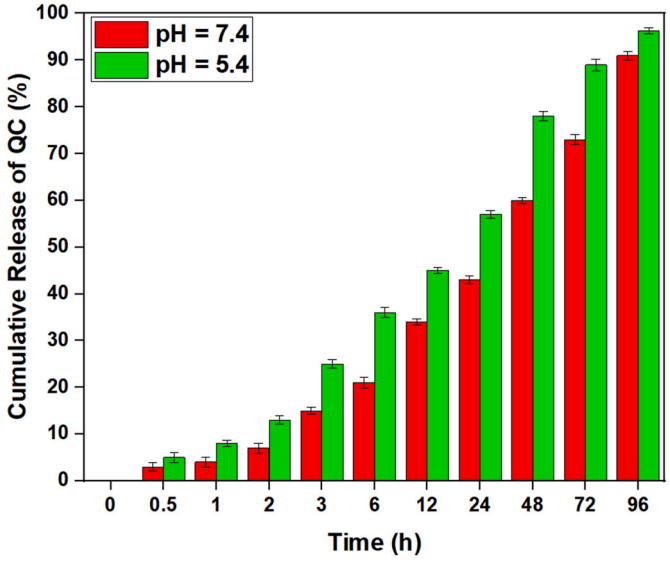

Fig. 7. Cumulative release curve for QC in acidic and neutral environments.

system (as a controlling membrane) along with SPAN 80 surfactant (as a stabilizing agent) help to tailor the release of QC, even after dissociation of nanocomposite structure.

3.7. Drug release kinetic modeling

The drug release data obtained from the dialysis method were fitted to different models in order to identify the best kinetic model to describe the release of QC from nanoparticles. The tested kinetic models were zero-order, first-order, Higuchi, Korsmeyer-Peppas, and Hixson-Crowell. By comparing R^2 values for the different models (Table 2), it was found that Higuchi and first-order model best describe the drug release kinetics in neutral and acidic medium, respectively. Figs. 8–12 show the drug release data fitted to the five abovementioned models.

According to R^2 values, Higuchi model is recognized as the best descriptive model for QC release in neutral environment ($R^2 = 0.9928$). In this model, the porous environment of the nanocarrier is divided in two regions: inner and outer region. While the drug is dissolved in the outer region, the opposite is true for the inner region. The following assumptions are appliable when Higuchi model is considered accurate: (1) Drug particles diameter are negligible compared to thickness of the surrounding walls (2) Drug diffusivity is constant (3) Swelling and dissociation of porous network is insignificant (4) The initial concentration of the drug is higher than its soluble capacity (5) Diffusion of drug molecules takes place in one dimension. The mathematical formulation for this model is as follows: $Q = A\sqrt{D(2C - C_s)C_s t}$. In this equation, Q, D, C, A, and C_s stand for the amount of released drug at time t, the diffusion coefficient of the drug molecules in the matrix substance, the drug initial concentration, the area and the drug solubility, respectively [51,52].

Table 2
Equations and R squared values for different kinetic models of drug release data.

Model	Equation	R^2
First-order (pH = 7.4)	$Ln\left(1 - \frac{M_t}{M_\infty}\right) = 4.5694 - 0.0218t$	0.9604
First-order (pH = 5.4)	$Ln\left(1 - \frac{M_t}{M_\infty}\right) = 4.5047 - 0.0316t$	0.9888
Zero-order (pH = 7.4)	$C_t = 0.9054t + 10.139$	0.9359
Zero-order (pH = 5.4)	$C_t = 0.9675t + 17.85$	0.8578
Korsmeyer-Peppas (pH = 7.4)	$Ln\left(\frac{M_t}{M_\infty}\right) = 1.6926 + 0.6391\ Ln(t)$	0.9604
Korsmeyer-Peppas (pH = 5.4)	$Ln\left(\frac{M_t}{M_\infty}\right) = 2.3815 + 0.5135\ Ln(t)$	0.9453
Hixson-Crowell (pH = 7.4)	$\left(1 - \frac{M_t}{M_\infty}\right)^{\frac{1}{3}} = 4.5286 - 0.0242t$	0.9771
Hixson-Crowell (pH = 5.4)	$\left(1 - \frac{M_t}{M_\infty}\right)^{\frac{1}{3}} = 4.3995 - 0.0308t$	0.9742
Higuchi (pH = 7.4)	$Q = 9.2744t^{0.5} - 2.5558$	0.9928
Higuchi (pH = 5.4)	$Q = 10.254t^{0.5} + 3.0081$	0.9761

On the other hand, the first-order model had the highest R^2 value in acidic medium. This indicates that the best kinetic model for QC release in acidic medium differs from that in neutral medium. First-order model is used to describe the dissolution of drug particles in pharmaceutical dosage forms such as those containing water-soluble drugs within porous networks. The mathematical formulation of this model is as follows: $\frac{dC}{dt} = -KC$, where K is the first-order rate constant [51].

3.8. Mechanism of cellular internalization

In section 3.1, an average zeta potential value of 51 mV was calculated for our final formulation. Although such polar nature might inhibit our highly charged nanoparticles from penetrating the lipid-based cellular membrane, possible electrostatic affinity between positively-charged nanoparticles and negatively-charged phosphate groups of phospholipids in the cellular membrane could increase residence time of nanoparticles within the membrane and provide enough contact time for Clathrin-Caveoun independent endocytosis. Also, previous studies on mechanism of cellular uptake of PLGA nanoparticles by U87 cells has verified clathrin-mediated endocytosis of polymeric nanoparticles by these cells [53]. Since our nanocomposite and PLGA nanoparticles are both copolymers with similar functional groups, it is expected that clathrin-mediated endocytosis is also the responsible for cellular internalization. However, no practical tests were carried out to verify these claims.

3.9. MTT assay

MTT assay was applied to assess the cytotoxicity and antineoplastic efficacy of PVP, PVP/PVA, PVP/PVA/TiO_2, PVP/PVA/TiO_2/QC against U87 cell line and compare its performance with the free drug. For this purpose, the different samples were incubated with the cancerous cell line for 24 h and the cell viability percentage was calculated (Fig. 13). Similar experiments were carried out with non-cancerous L929 fibroblast cell line to estimate potential side effects of the prepared samples and get insight about their biocompatibility. Moreover, a negative control group was incubated for both cell lines to confirm natural behavior of cell lines.

Cell viability percentages for the control group of both cell lines was almost 100% which verifies their quality. Except for this group, all the tested materials induced more cytotoxic effects on cancerous cells compared with fibroblast cells. It is evident from Fig. 13 that cross-linking of PVP and PVA partially ameliorates cytotoxicity of PVP for both cell lines. The final formulation of the nanoparticles (PVP/PVA/TiO_2/QC) decreases cell viability of U87 cells to 61%, whereas for free QC is 74%. This result is an obvious indicator of the superior antitumor activity of our drug delivery system compared to the free drug. High encapsulation efficiency offered by the nanocomposite and prolonged release time arising from the double emulsion has led to enhanced therapeutic efficiency of entrapped QC compared to its free form.

Regarding L929 cells, none of the synthesized samples showed a significant reduction of cell viability when compared with the control, which corroborates their good biocompatibility. Thus, 96% of these cells survived 24 h of incubation with QC-loaded nanoparticles. This is in agreement with previous studies that indicated good biocompatibility of positively charged nanoparticles [57,58]. Furthermore, high positive surface charge can result in electrostatic affinity between nanoparticles and negatively charged cellular membrane. Hence, cellular uptake of

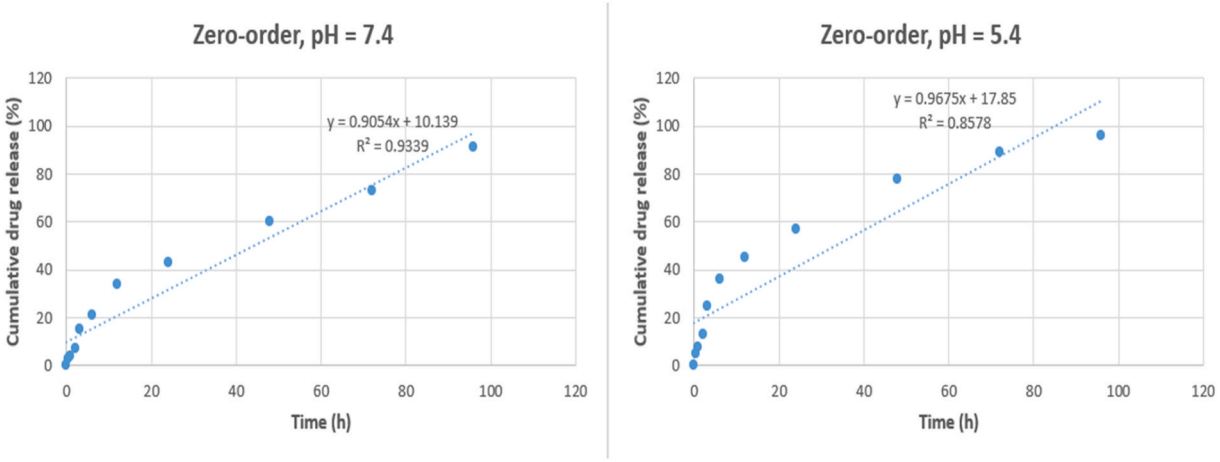

Fig. 8. QC release data fitted to zero-order model.

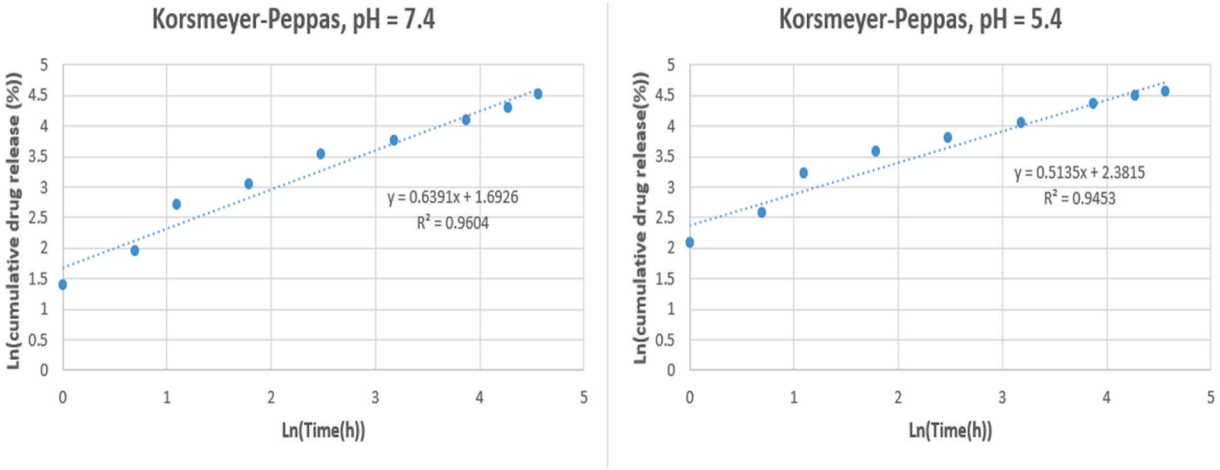

Fig. 9. QC release data fitted to Korsmeyer-Peppas model.

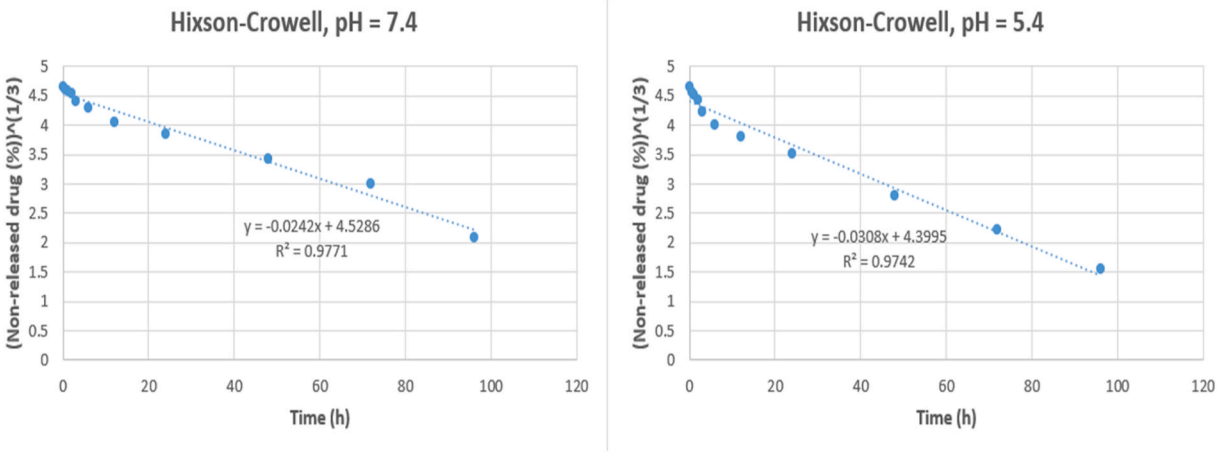

Fig. 10. QC release data fitted to Hixson-Crowell model.

nanoparticles will be improved. The pH-responsivity of the PVP/PVA/TiO_2 nanocomposite is responsible for this behavior, as lower amount of QC is released in the neutral environment of L929 cells compared to the acid environment of U87 cells. This result is highly suitable as it proves reduced side effects of the fabricated nanocarriers. Also, L929 cell viability for free QC is 13% lower than that of QC-loaded nanoparticles which further validates the effectiveness of the designed drug delivery system.

Regarding *in vivo* studies, previously published works on polymeric nanocarriers for QC delivery showed the potential of this class of nanostructures for improving its therapeutic efficiency. El-Gogary et al. [54] developed PEG-conjugated PLGA nanocapsules for QC delivery. *In*

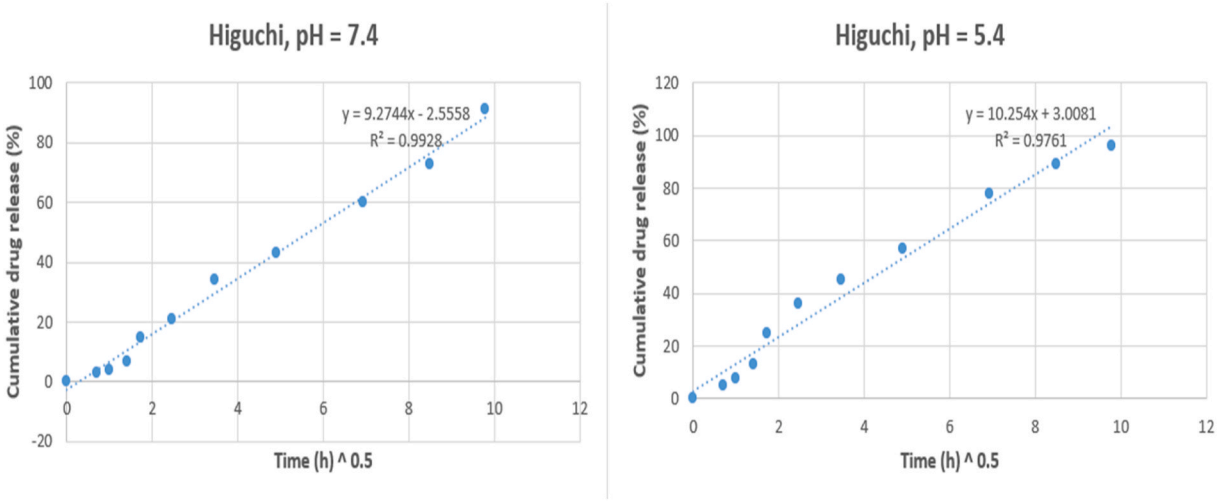

Fig. 11. QC release data fitted to Higuchi model.

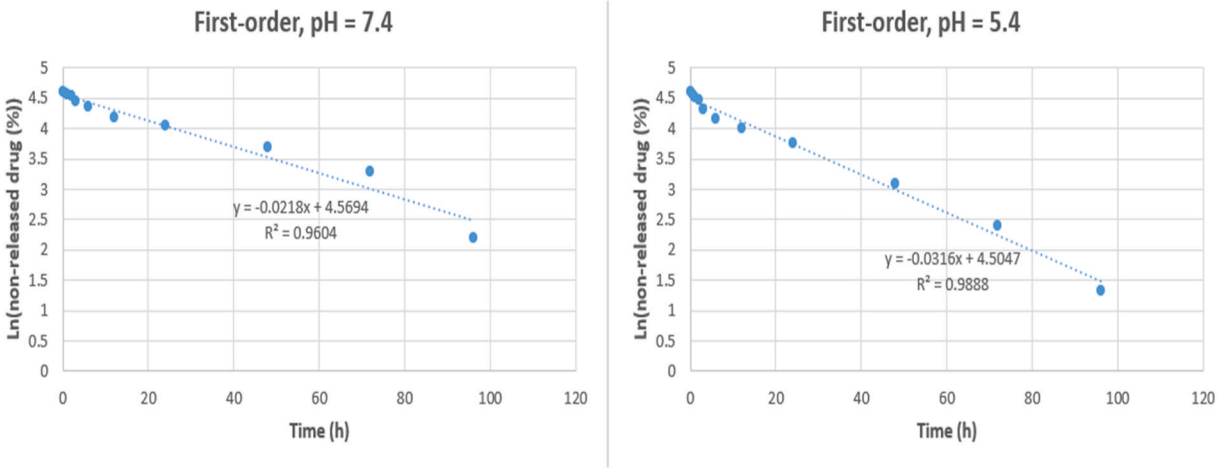

Fig. 12. QC release data fitted to first-order model.

vivo tests using tumor-bearing mice model demonstrated noticeable accumulation of the drug at the tumor site. However, significant accumulation of QC in the lung was observed as well. In another study, Pang and colleagues [55] developed bioconjugates of QC and hyaluronic acid and conducted *in vivo* experiments using tumor-bearing mice model. The percentage of reduction in tumor size was much higher in the group treated with the new formulation (62%) compared to the control group treated with free QC (25%). *In vivo* studies with PVP/PVA/TiO2/QC will be carried out in the future prior to their potential use in biomedical applications.

3.10. Flow cytometry

To confirm the results obtained from MTT assay and further analyze the antineoplastic activity of the nanocarrier, flow cytometry test was performed using U87 cell line. The test was performed for PVP, PVP/PVA, PVP/PVA/TiO_2, PVP/PVA/TiO_2/QC, and free QC (Fig. 14). As mentioned in the experimental section, the four quadrants in Fig. 14 stand for necrotic death (Q1), late apoptotic death (Q2), early apoptotic death (Q3), and viability of cells. In case of PVP, severe cytotoxic effects were observed with less than 50% of cells surviving incubation. Cross-linking of PVP and PVA attenuated the cytotoxicity of PVP significantly and the cell viability increased to 75.1%. This result was consistent with MTT assay findings. However, the incorporation of TiO_2 nanoparticles within the polymeric structure caused a significant rise in early apoptotic death rate which is an evident indicator of cytotoxic property of TiO_2. This finding is consistent with former literature reports [56]. The experiment with the final formulation consisting of double emulsion-entrapped QC-loaded nanocomposite (PVP/PVA/TiO_2/QC) demonstrated the highest level of early apoptosis death rate among the incubated samples. While the early apoptosis death rate for QC-loaded nanocarrier was 60.9%, for free QC was about 14.6%. Moreover, late apoptotic death share of QC-loaded nanocarriers was also higher than that of free QC (5.31% and 2.08%, respectively). This outcome can be attributed to the gradual release profile of QC, which is associated with the double emulsion and the broad chemical interactions of QC and building components of the nanocomposite. These factors contribute to extend the release period of QC. The higher effectiveness of QC-loaded nanoparticles compared to free QC in destroying U87 cells is in agreement with MTT assay results.

4. Conclusion

Low bioavailability, unstable form, and non-specific therapeutic behavior limit the efficiency of QC as an antineoplastic agent. In light of this fact, drug delivery systems fabricated for QC need to have a gradual release profile, high capacity for encapsulating the necessary amount of the drug, and sensitivity towards a stimulus in order to release QC on

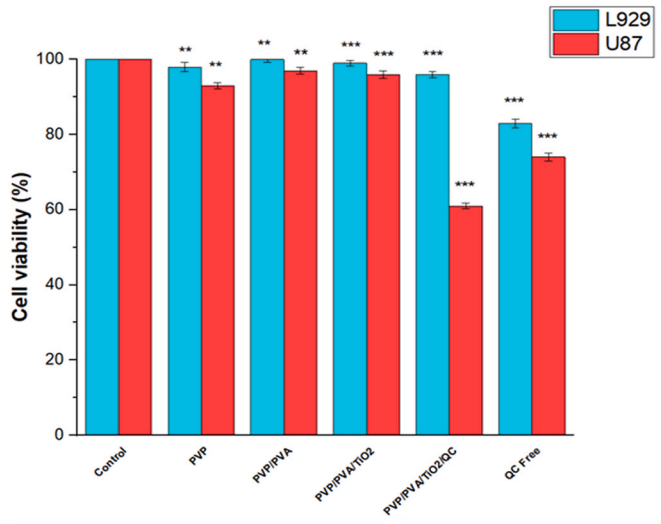

Fig. 13. MTT assay results after 24 h for L929 and U87 cells. Experiments were performed in triplicate and the results are shown in the form of mean ± SEM. Based statistical analysis, the sign ** represents difference between the relative sample and control group with significance below 0.01 ($p < 0.01$). The sign *** represents difference between the relative sample and control group with significance below 0.001 ($p < 0.001$).

demand. Since pH values for cancerous and normal tissues are meaningfully different, the use of a pH-responsive formulation is a smart approach towards targeted QC delivery. Herein, a QC-loaded nanocomposite composed of PVP/PVA/TiO_2 entrapped in a double emulsion of water-in-oil-in-water was synthesized. The use of TiO_2 nanoparticles with high surface area contributes to improve the loading and encapsulation efficiency of the nanocarrier. FTIR analysis revealed strong chemical interactions between QC and the nanocomposite components. These interactions together with the use of double emulsion provided a sustained release profile for the therapeutic cargo. Moreover, the comparison of the release patterns at pH values of 7.4 and 5.4 revealed that protonation of carbonyl (PVP) and hydroxyl (PVA and QC) groups of the QC-loaded nanocomposite at low pH causes disruption of the nanocarrier structure and better release of the drug. In vitro release experiments revealed that this formulation perfectly leverages the difference between the pH value of normal and cancerous tissues to control the release of its cargo. The gradual release profile and pH-responsiveness of the nanocarrier can resolve issues such as insufficient biological half-life and inefficient biodistribution of QC. MTT assay using U87 cell line demonstrated superior antitumor activity of QC-loaded nanoparticles compared to free QC, attributed to a gradual release of QC resulting from the double emulsion system that induced more apoptosis, and was further confirmed using flow cytometry test. MTT assay with L929 cell line showed that the fabricated drug-loaded nanoparticles have less cytotoxic effects against the fibroblast cells than the free QC, thus proving their high biocompatibility. Overall, the developed nanocarrier successfully circumvented many issues which limit QC therapeutic efficiency.

Funding

Financial support from the Community of Madrid within the framework of the multi-year agreement with the University of Alcalá in the line of action "Stimulus to Excellence for Permanent University Professors", Ref. EPU-INV/2020/012, is gratefully acknowledged.

Credit author statement

Mohammad Mahdi Eshaghi, Mehrab Pourmadadi: Writing—original draft. Abbas Rahdar: Conceptualization. Abbas Rahdar, Mehrab Pourmadadi, Ana M. Díez-Pascual: Writing – review & editing. Abbas Rahdar, Ana M. Díez-Pascual: Supervision.

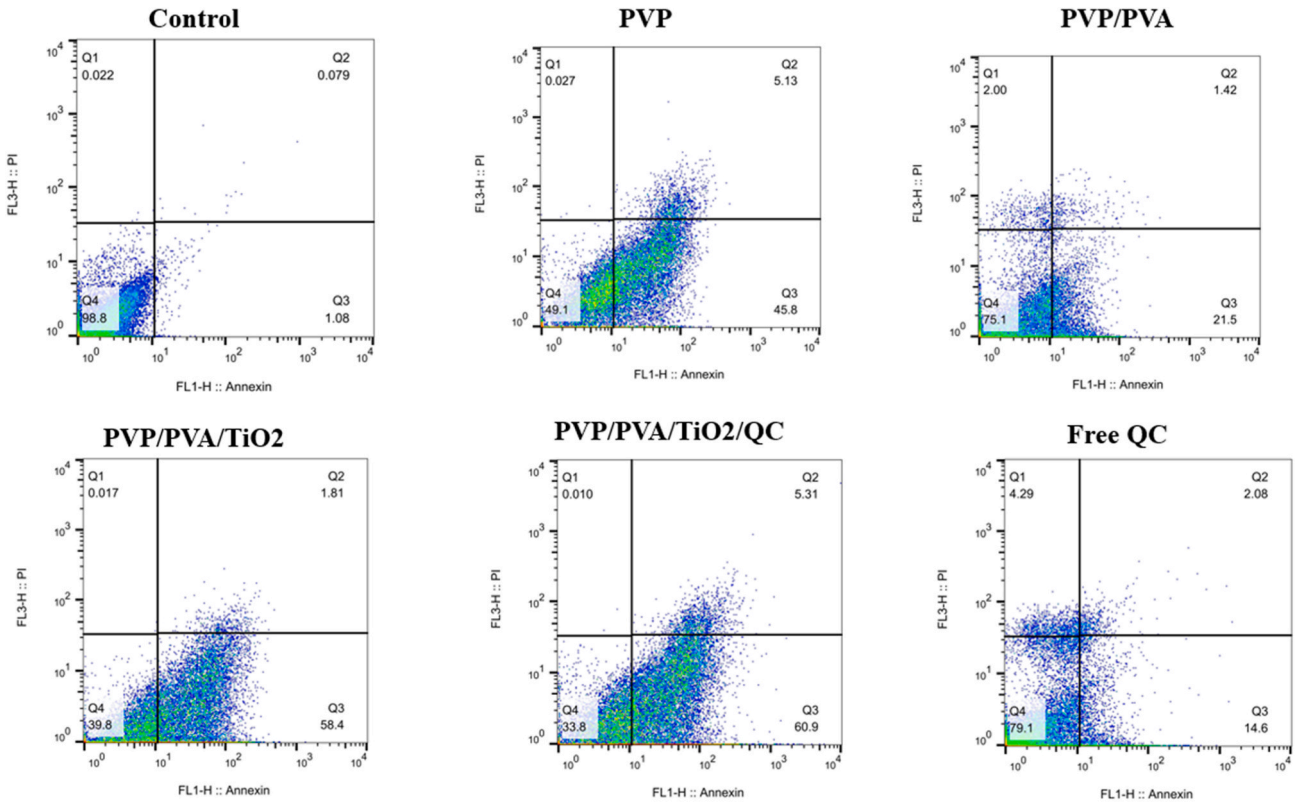

Fig. 14. Flow cytometry results using U87 cell line for PVP, PVP/PVA, PVP, PVA/TiO_2, PVP/PVA/TiO_2/QC, and free QC.

Declaration of competing interest

The authors declare that they have no known competing financial interests or personal relationships that could have appeared to influence the work reported in this paper.

Data availability

Data will be made available on request.

References

[1] R.L. Siegel, K.D. Miller, A. Jemal, Cancer statistics, 2019, CA: Cancer. J. Clinicians. 69 (2019) 7–34.

[2] C. Pucci, C. Martinelli, G. Ciofani, Innovative approaches for cancer treatment: current perspectives and new challenges, Ecancermedicalscience 13 (2019).

[3] M. Pourmadadi, M.M. Eshaghi, E. Rahmani, N. Ajalli, S. Bakhshi, H. Mirkhaef, M. V. Lasemi, A. Rahdar, R. Behzadmehr, A.M. Díez-Pascual, Cisplatin-loaded nanoformulations for cancer therapy: a comprehensive review, J. Drug Deliv. Sci. Technol. 77 (2022), 103928, https://doi.org/10.1016/j.jddst.2022.103928.

[4] Kashyap, D., H.S. Tuli, M.B. Yerer, A. Sharma, K. Sak, S. Srivastava, A. Pandey, V.K. Garg, G. Sethi, and A. Bishayee, Natural Product-Based Nanoformulations for Cancer Therapy: Opportunities and Challenges, vol. 69 (Year) 5-23.

[5] M. Ezzati, B. Yousefi, K. Velaei, A. Safa, A review on anti-cancer properties of Quercetin in breast cancer, Life Sci. 248 (2020), 117463.

[6] M. Reyes-Farias, C. Carrasco-Pozo, The anti-cancer effect of quercetin: molecular implications in cancer metabolism, Int. J. Mol. Sci. 20 (2019) 3177.

[7] S.Q. Chen, C. Wang, S. Tao, Y.X. Wang, F.Q. Hu, H. Yuan, Rational design of redox-responsive and P-gp-Inhibitory lipid nanoparticles with high entrapment of paclitaxel for tumor therapy, Adv. Healthcare Mater. 7 (2018), 1800485.

[8] C. Caro, M. Pourmadadi, M.M. Eshaghi, E. Rahmani, S. Shojaei, A.C. Paiva-Santos, A. Rahdar, R. Behzadmehr, M.L. García-Martín, A.M. Díez-Pascual, Nanomaterials loaded with Quercetin as an advanced tool for cancer treatment, J. Drug Deliv. Sci. Technol. 78 (2022), 103938, https://doi.org/10.1016/j.jddst.2022.103938.

[9] M. Pourmadadi, P. Abbasi, M.M. Eshaghi, A. Bakhshi, A.-L. Ezra Manicum, A. Rahdar, S. Pandey, S. Jadoun, A.M. Díez-Pascual, Curcumin delivery and co-delivery based on nanomaterials as an effective approach for cancer therapy, J. Drug Deliv. Sci. Technol. 78 (2022), 103982, https://doi.org/10.1016/j.jddst.2022.103982.

[10] Y.K. Sung, S.W. Kim, Recent advances in polymeric drug delivery systems, Biomater. Res. 24 (2020) 1–12.

[11] P. Ghasemiyeh, S. Mohammadi-Samani, Hydrogels as drug delivery systems; pros and cons, Trend. Pharmaceut. Sci. 5 (2019) 7–24.

[12] D. Qureshi, S.K. Nayak, S. Maji, A. Anis, D. Kim, K. Pal, Environment sensitive hydrogels for drug delivery applications, Eur. Polym. J. 120 (2019), 109220.

[13] X. Fang, Y. Liu, M. Zhang, S. Zhou, P. Cui, H. Hu, P. Jiang, C. Wang, L. Qiu, J. Wang, Glucose oxidase loaded thermosensitive hydrogel as an antibacterial wound dressing, J. Drug Deliv. Sci. Technol. 76 (2022), 103791.

[14] M. Rasoulzadeh, H. Namazi, Carboxymethyl cellulose/graphene oxide bio-nanocomposite hydrogel beads as anticancer drug carrier agent, Carbohydr. Polym. 168 (2017) 320–326.

[15] N. Mulchandani, N. Shah, T. Mehta, Synthesis of chitosan-polyvinyl alcohol copolymers for smart drug delivery application, Polym. Polym. Compos. 25 (2017) 241–246.

[16] M. Kurakula, G.K. Rao, Pharmaceutical assessment of polyvinylpyrrolidone (PVP): as excipient from conventional to controlled delivery systems with a spotlight on COVID-19 inhibition, J. Drug Deliv. Sci. Technol. 60 (2020), 102046.

[17] C.F. Vecchi, G.B. Cesar, P.R.d. Souza, W. Caetano, M.L. Bruschi, Mucoadhesive polymeric films comprising polyvinyl alcohol, polyvinylpyrrolidone, and poloxamer 407 for pharmaceutical applications, Pharmaceut. Dev. Technol. 26 (2021) 138–149.

[18] S. Mura, J. Nicolas, P. Couvreur, Stimuli-responsive nanocarriers for drug delivery, Nat. Mater. 12 (2013) 991–1003, https://doi.org/10.1038/nmat3776.

[19] R. Jia, L. Teng, L. Gao, T. Su, L. Fu, Z. Qiu, Y. Bi, Advances in multiple stimuli-responsive drug-delivery systems for cancer therapy, Int. J. Nanomed. 16 (2021) 1525.

[20] E. Rahmani, M. Pourmadadi, S.A. Ghorbanian, F. Yazdian, H. Rashedi, M. Navaee, Preparation of a pH-responsive chitosan-montmorillonite-nitrogen-doped carbon quantum dots nanocarrier for attenuating doxorubicin limitations in cancer therapy, Eng. Life Sci. 22 (2022) 634–649, https://doi.org/10.1002/elsc.202200016.

[21] Y.J. Zhu, F. Chen, pH-responsive drug-delivery systems, Chem.–Asian J. 10 (2015) 284–305.

[22] M. Pourmadadi, M. Ahmadi, M. Abdouss, F. Yazdian, H. Rashedi, M. Navaei-Nigjeh, Y. Hesari, The synthesis and characterization of double nanoemulsion for targeted Co-Delivery of 5-fluorouracil and curcumin using pH-sensitive agarose/chitosan nanocarrier, J. Drug Deliv. Sci. Technol. 70 (2022), 102849, https://doi.org/10.1016/j.jddst.2021.102849.

[23] K. Madhusudana Rao, K.S.V. Krishna Rao, G. Ramanjaneyulu, C.-S. Ha, Curcumin encapsulated pH sensitive gelatin based interpenetrating polymeric network nanogels for anti cancer drug delivery, Int. J. Pharm. 478 (2015) 788–795, https://doi.org/10.1016/j.ijpharm.2014.12.001.

[24] M. Hamidi, A. Azadi, P. Rafiei, Hydrogel nanoparticles in drug delivery, Adv. Drug Deliv. Rev. 60 (2008) 1638–1649.

[25] A. Servant, V. Leon, D. Jasim, L. Methven, P. Limousin, E.V. Fernandez-Pacheco, M. Prato, K. Kostarelos, Graphene-based electroresponsive scaffolds as polymeric implants for on-demand drug delivery, Adv. Healthcare Mater. 3 (2014) 1334–1343.

[26] A. Ahsan, W.-X. Tian, M.A. Farooq, D.H. Khan, An overview of hydrogels and their role in transdermal drug delivery, Int. J. Polym. Mater. Polym. Biomater. 70 (2021) 574–584.

[27] T.R. Hoare, D.S. Kohane, Hydrogels in drug delivery: progress and challenges, Polymer 49 (2008) 1993–2007.

[28] F. Song, X. Li, Q. Wang, L. Liao, C. Zhang, Nanocomposite hydrogels and their applications in drug delivery and tissue engineering, J. Biomed. Nanotechnol. 11 (2015) 40–52.

[29] H. Zhang, C. Wang, B. Chen, X. Wang, Daunorubicin-TiO2 nanocomposites as a "smart" pH-responsive drug delivery system, Int. J. Nanomed. 7 (2012) 235.

[30] Z. Aayanifard, T. Alebrahim, M. Pourmadadi, F. Yazdian, H.S. Dinani, H. Rashedi, M. Omidi, Ultra pH-sensitive detection of total and free prostate-specific antigen using electrochemical aptasensor based on reduced graphene oxide/gold nanoparticles emphasis on TiO2/carbon quantum dots as a redox probe, Eng. Life Sci. 21 (2021) 739–752, https://doi.org/10.1002/elsc.202000118.

[31] K. Ghosal, C. Agatemor, Z. Špitálsky, S. Thomas, E. Kny, Electrospinning tissue engineering and wound dressing scaffolds from polymer-titanium dioxide nanocomposites, Chem. Eng. J. 358 (2019) 1262–1278.

[32] S. Haseli, M. Pourmadadi, A. Samadi, F. Yazdian, M. Abdouss, H. Rashedi, M. Navaei-Nigjeh, A novel pH-responsive nanoniosomal emulsion for sustained release of curcumin from a chitosan-based nanocarrier: emphasis on the concurrent improvement of loading, sustained release, and apoptosis induction, Biotechnol. Prog. (2022), e3280, https://doi.org/10.1002/btpr.3280 n/a.

[33] P.I. Febriyenti, E. Zaini, F. Ismed, H. Lucida, Preparation and characterization of quercetin-polyvinylpyrrolidone K-30 spray dried solid dispersion, J Pharm Pharmacogn Res 8 (2020) 127–134.

[34] T. He, H. Wang, Z. Chen, S. Liu, J. Li, S. Li, Natural quercetin AIEgen composite film with antibacterial and antioxidant properties for in situ sensing of Al3+ residues in food, detecting food spoilage, and extending food storage times, ACS Appl. Bio Mater. 1 (2018) 636–642.

[35] J. Ahmad, K. Deshmukh, M.B. Hägg, Influence of TiO2 on the chemical, mechanical, and gas separation properties of polyvinyl alcohol-titanium dioxide (PVA-TiO2) nanocomposite membranes, Int. J. Polym. Anal. Char. 18 (2013) 287–296.

[36] M. Rajabzadeh-Khosroshahi, M. Pourmadadi, F. Yazdian, H. Rashedi, M. Navaei-Nigjeh, B. Rasekh, Chitosan/agarose/graphitic carbon nitride nanocomposite as an efficient pH-sensitive drug delivery system for anticancer curcumin releasing, J. Drug Deliv. Sci. Technol. 74 (2022), 103443, https://doi.org/10.1016/j.jddst.2022.103443.

[37] M. Chouaibi, J. Mejri, L. Rezig, K. Abdelli, S. Hamdi, Experimental study of quercetin microencapsulation using water-in-oil-in-water (W1/O/W2) double emulsion, J. Mol. Liq. 273 (2019) 183–191.

[38] W. Zheng, A water-in-oil-in-oil-in-water (W/O/O/W) method for producing drug-releasing, double-walled microspheres, Int. J. Pharm. 374 (2009) 90–95.

[39] J. Ceramella, A.-C. Groo, D. Iacopetta, L. Séguy, A. Mariconda, F. Puoci, C. Saturnino, F. Leroy, M. Since, P. Longo, A winning strategy to improve the anticancer properties of Cisplatin and Quercetin based on the nanoemulsions formulation, J. Drug Deliv. Sci. Technol. 66 (2021), 102907.

[40] J.A.A. Júnior, J.B. Baldo, The behavior of zeta potential of silica suspensions, New J. Glass Ceram. 4 (2014) 29.

[41] N. Rajeswari, S. Selvasekarapandian, S. Karthikeyan, M. Prabu, G. Hirankumar, H. Nithya, C. Sanjeeviraja, Conductivity and dielectric properties of polyvinyl alcohol–polyvinylpyrrolidone poly blend film using non-aqueous medium, J. Non-Cryst. Solids 357 (2011) 3751–3756.

[42] J.-Y. Zhang, I.W. Boyd, B. O'sullivan, P. Hurley, P. Kelly, J.-P. Senateur, Nanocrystalline TiO2 films studied by optical, XRD and FTIR spectroscopy, J. Non-Cryst. Solids 303 (2002) 134–138.

[43] B. Erdem, R.A. Hunsicker, G.W. Simmons, E.D. Sudol, V.L. Dimonie, M.S. El-Aasser, XPS and FTIR surface characterization of TiO2 particles used in polymer encapsulation, Langmuir 17 (2001) 2664–2669.

[44] Y.-H. Wu, D.-G. Yu, H.-P. Li, X.-Y. Wu, X.-Y. Li, Medicated structural PVP/PEG composites fabricated using coaxial electrospinning, E-Polymers 17 (2017) 39–44.

[45] T. Theivasanthi, M. Alagar, Titanium Dioxide (TiO2) Nanoparticles XRD Analyses: an Insight, 2013 arXiv preprint arXiv:1307.1091.

[46] M. Rossi, L.F. Rickles, W.A. Halpin, The crystal and molecular structure of quercetin: a biologically active and naturally occurring flavonoid, Bioorg. Chem. 14 (1986) 55–69, https://doi.org/10.1016/0045-2068(86)90018-0.

[47] T. Wang, C. Wu, T. Li, G. Fan, H. Gong, P. Liu, Y. Yang, L. Sun, Comparison of two nanocarriers for quercetin in morphology, loading behavior, release kinetics and cell inhibitory activity, Mater. Express. 10 (2020) 1589–1598.

[48] R. Baksi, D.P. Singh, S.P. Borse, R. Rana, V. Sharma, M. Nivsarkar, In vitro and in vivo anticancer efficacy potential of Quercetin loaded polymeric nanoparticles, Biomed. Pharmacother. 106 (2018) 1513–1526.

[49] S. Sunoqrot, L. Abujamous, pH-sensitive polymeric nanoparticles of quercetin as a potential colon cancer-targeted nanomedicine, J. Drug Deliv. Sci. Technol. 52 (2019) 670–676.

[50] A. Samadi, M. Pourmadadi, F. Yazdian, H. Rashedi, M. Navaei-Nigjeh, Ameliorating quercetin constraints in cancer therapy with pH-responsive agarose-polyvinylpyrrolidone-hydroxyapatite nanocomposite encapsulated in double nanoemulsion, Int. J. Biol. Macromol. 182 (2021) 11–25.

[51] S. Dash, P.N. Murthy, L. Nath, P. Chowdhury, Kinetic modeling on drug release from controlled drug delivery systems, Acta Pol. Pharm. 67 (2010) 217–223.
[52] D. Paul, Elaborations on the Higuchi model for drug delivery, Int. J. Pharm. 418 (2011) 13–17.
[53] Y. Malinovskaya, P. Melnikov, V. Baklaushev, A. Gabashvili, N. Osipova, S. Mantrov, Y. Ermolenko, O. Maksimenko, M. Gorshkova, V. Balabanyan, Delivery of doxorubicin-loaded PLGA nanoparticles into U87 human glioblastoma cells, Int. J. Pharm. 524 (2017) 77–90.
[54] R.I. El-Gogary, N. Rubio, J.T.-W. Wang, W.T. Al-Jamal, M. Bourgognon, H. Kafa, M. Naeem, R. Klippstein, V. Abbate, F. Leroux, S. Bals, G. Van Tendeloo, A. O. Kamel, G.A.S. Awad, N.D. Mortada, K.T. Al-Jamal, Polyethylene glycol conjugated polymeric nanocapsules for targeted delivery of quercetin to folate-expressing cancer cells in vitro and in vivo, ACS Nano 8 (2014) 1384–1401, https://doi.org/10.1021/nn405155b.
[55] X. Pang, Z. Lu, H. Du, X. Yang, G. Zhai, Hyaluronic acid-quercetin conjugate micelles: synthesis, characterization, in vitro and in vivo evaluation, Colloids Surf. B Biointerfaces 123 (2014) 778–786, https://doi.org/10.1016/j.colsurfb.2014.10.025.
[56] I.-S. Kim, M. Baek, S.-J. Choi, Comparative cytotoxicity of Al2O3, CeO2, TiO2 and ZnO nanoparticles to human lung cells, J. Nanosci. Nanotechnol. 10 (2010) 3453–3458.